JACS
JOURNAL OF THE AMERICAN CHEMICAL SOCIETY
Article
pubs.acs.org/JACS

Bioinspired Water-Enhanced Mechanical Gradient Nanocomposite Films That Mimic the Architecture and Properties of the Squid Beak

Justin D. Fox,[†] Jeffrey R. Capadona,[‡,§] Paul D. Marasco,[§] and Stuart J. Rowan*[,†,‡,⊥]

[†]Department of Macromolecular Science and Engineering, Case Western Reserve University, 2100 Adelbert Road, Kent Hale Smith Building, Cleveland, Ohio 44106-7202, United States

[‡]Department of Biomedical Engineering, Case Western Reserve University, 2071 Martin Luther King Jr. Drive, Wickenden Building, Cleveland, Ohio 44106, United States

[§]Advanced Platform Technology Center, Louis Stokes Cleveland Department of Veterans Affairs Medical Center, 10701 East Boulevard 151 W/APT, Cleveland, Ohio 44106-1702, United States

[⊥]Department of Chemistry, Case Western Reserve University, Cleveland, Ohio 44106, United States

Supporting Information

ABSTRACT: Inspired by the water-enhanced mechanical gradient character of the squid beak, we herein report a nanocomposite that mimics both the architecture and properties of this interesting natural material. Similar to the squid beak, we have developed nanocomposites where the degree of cross-linking is controlled along the length of the film. In this study, we utilized tunicate cellulose nanocrystals as the nanofiller that are functionalized with allyl moieties. Using photoinduced thiol−ene chemistry, we have been able to cross-link the CNC nanofiller. In the dry state where strong CNC interactions can occur, only a small mechanical contrast is observed between the cross-linked and uncross-linked samples. However, when the films are exposed to water, which "switches off" the noncovalent CNC interactions, a significant mechanical contrast is observed between the same films. For example, at 20 wt % CNC (in the dry film), an increase in wet modulus from 60 to 300 MPa (~500% increase) is observed after photoirradiation. Furthermore, we show that the wet modulus can be controlled by altering the UV exposure time which allows access to mechanical gradient films.

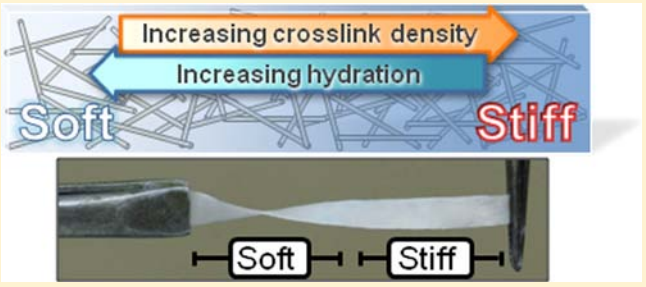

INTRODUCTION

Biological materials often demonstrate a range of remarkable physical properties[1] that have evolved for a specific application, such as defense, lightweight, adhesion, impact resistance, and so forth. To obtain such properties, nature has often utilized nanocomposites, examples of which include nacre[2] (which shows excellent toughness) and the inner dermis of the sea cucumber[3] (which exhibits mechanical adaptability). The squid beak is another interesting natural nanocomposite that has evolved to function as a mechanical bridge between the sharp, stiff tip of the beak (rostrum, Figure 1a)[4] and the soft connecting muscle tissues (buccal envelope). The rostrum is of interest as it is one of the hardest entirely organic (i.e., nonmineralized) materials known.[5,6] The remainder of the squid's beak (the wing) performs the remarkable task of insulating the soft buccal envelope from the high interfacial stresses generated at the rostrum during feeding. The large mechanical mismatch is bridged by a gradient in stiffness that runs from the relatively compliant wing edge (elastic modulus ca. 50 MPa) to the razor sharp rostrum (elastic modulus ca. 5 GPa) when in its natural wet state.[7] In fact, gradients are found frequently in nature at the interface of two mechanically dissimilar materials.[8] Other than the squid beak, mechanical gradients occur in crustacean exoskeletons,[9] polychelate jaws,[10] teeth,[11−13] and in the mussel byssus.[10]

Gradient materials are attracting attention in the fields of polymer science[14] and metallurgy.[15] Suresh[16] has outlined the advantages of mechanical gradients in materials to include increased distribution of interfacial mechanical and thermal stress, improvements in bonding of dissimilar mechanical components, reduced contact deformation and damage, elimination of stress singularities and improved fracture toughness. In addition, chemical and functional gradient surfaces are being investigated to control the movement of a range of components (e.g., water drops, dendrimers and cells)[17] or to control surface assembly of block copolymers in polymer thin films.[18]

Studies performed by Waite, Zok and co-workers[4] suggest that the mechanical gradient of the squid beak, which is composed of a fibrous (ca. 30 nm fiber diameter) chitin network (Figure 1b)[4] embedded within a biopolymer matrix,

Received: January 9, 2013
Published: March 26, 2013

   dx.doi.org/10.1021/ja4002713 | J. Am. Chem. Soc. 2013, 135, 5167−5174

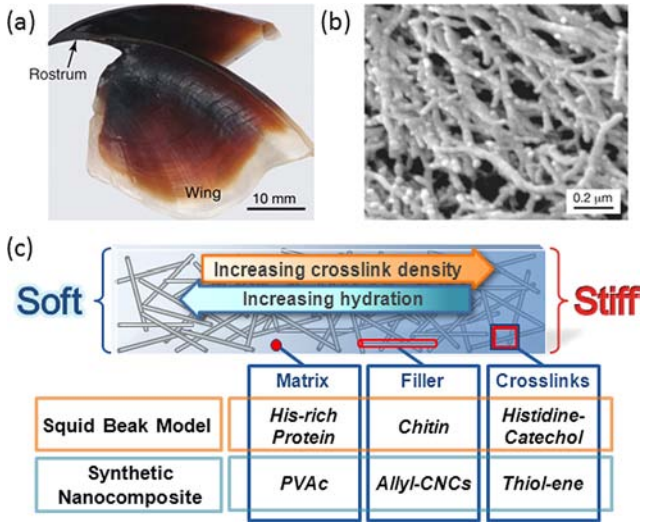

Figure 1. Pictures of (a) a split beak of the Humboldt Squid *Dosidicus gigas* after removal from the buccal mass showing the relation of the wing to the rostrum and (b) a high-magnification scanning electron image of the chitin fiber network in the rostrum after alkaline peroxidation of the beak. Both a and b are from the work of Zok, Waite and co-workers ref 4. Reprinted with permission from AAAS. (c) Schematic representation of water-enhanced mechanical gradient nanocomposite in the squid beak biomodel and the proposed synthetic biomimic.

correlates with a change in the cross-linking density along the length of the material (Figure 1c). From these studies, it was proposed that cross-linking occurs between the imidazole functionality of peptidyl-histidine residues and both low molecular weight and peptidyl (via L-DOPA residues) catechol moieties, suggesting that the cross-linking occurs predominantly within the biomatrix phase.[19] Di-, tri-, and tetra-histidine-catecholic adducts were identified, suggesting a high degree of cross-linking present in the mature squid beak. It is interesting to note that the mechanical gradient is greatly diminished if the beak is dehydrated (only ranging from an elastic modulus of 5−10 GPa) but in its natural hydrated state, the beak possesses a gradient in stiffness that spans 2 orders of magnitude (elastic modulus ranging from 50 MPa to 5 GPa). In this biocomposite, high covalent cross-link densities at the rostrum correspond with a high stiffness and, not coincidentally, the least water of hydration (ca. 15 wt %). Conversely, the wing of the beak (i.e., the base) contains fewer cross-links, more chitin fibers and consequently significantly more water (ca. 70 wt %). Therefore, the squid beak can be considered a nanocomposite with a hydration-enhanced stiffness gradient that is directed by cross-linking.

We have previously investigated stimuli-responsive nanocomposite materials[20] whose inspiration originated in the dynamic mechanical properties of the inner dermis of the sea cucumber. Using stiff cellulose nanocrystals (CNCs) as the filler, we have prepared a series of nanocomposites that exhibit dramatic softening upon exposure to water.[21] CNCs[22] are natural, nano-sized fibers that have attracted much interest in the past decade as a class of bioavailable nanomaterials[23] and as potential "green" nanofillers for a variety of polymer nanocomposites.[24−30] They can be isolated from a range of renewable materials including plants,[31−33] bacteria,[34] and tunicates.[35] Depending on the method of isolation and the biosource from which they are obtained, the width of the CNC ranges from 5 to 30 nm (similar to the chitin isolated from the squid beak) and their aspect ratio can vary from ca. 10 to 100. We have shown that water-responsive, mechanically adaptable CNC nanocomposites can be accessed from a variety of polymer matrices (including poly(vinyl acetate)),[21,36] polyacrylates,[37] poly(ethylene oxide-*co*-epichlorohydrin),[21] polybutadiene,[38] styrene-butadiene rubber[38] and polyurethane[39]) and using CNCs obtained from a variety of different biosources (including from tunicates, cotton[40] and microcrystalline cellulose[41]). In general, it has been proposed that when these nanocomposites are dry the CNCs form a reinforcing, percolating network (which may also be aided by matrix−CNC interactions) bound primarily by hydrogen bonding interactions. This percolating network then acts as a scaffold, transferring mechanical stresses across the sample,[42] resulting in stiff materials. Mechanical softening is achieved upon exposure to water on account of water diffusing into the matrix and competitively hydrogen bonding with the CNC surfaces which disrupts the stress-bearing CNC scaffold.

One of the attractive features of CNCs is the possibility to tailor their surface properties through functionalization of the surface hydroxyl groups. For example, recently we have shown that functionalizing the CNCs with either carboxylic acid or amine moieties allows access to pH-responsive mechanically dynamic materials.[43]

Building on this previous work and inspired by the squid beak biomodel, we hypothesized that if the water sensitive hydrogen bonding interactions critical to the CNC network were replaced with covalent cross-links, then the CNC−CNC scaffold would be permanently "switched on" which in turn would greatly reduce the amount of mechanical softening upon exposure to water. Furthermore, if we can control the degree of cross-linking across such a nanocomposite film, we should not only be able to access mechanical gradient films, but films that also experience an enhancement in the mechanical gradient contrast upon exposure to water, akin to what is observed in the squid beak (Figure 1).

Thus, we report herein our first attempt to mimic the water-enhanced mechanical gradient properties of the squid beak by utilizing photoinduced thiol−ene cross-linking of a tunicate CNC nanocomposite, where the degree of cross-linking can be controlled by the time of exposure to UV irradiation (Figure 2). In contrast with the predominantly intramatrix cross-linking proposed for the biomodel, this study investigates whether cross-linking just the rigid filler network would allow access to hydration-sensitive mechanical gradient films. To this end, we have designed a cross-linkable nanocomposite system (Figure 2) composed of alkene-functionalized CNCs, a small molecule tetra-thiol cross-linker (**1**) and a radical photoinitiator (**2**), embedded within a poly(vinyl acetate) (PVAc) matrix.

EXPERIMENTAL SECTION

Materials. All materials and reagents were used as-received or as-collected. Organic solvents and reagents were purchased from Sigma-Aldrich.

Synthesis of Allyl-Functionalized CNCs. CNCs were isolated from the mantles of sea tunicates after hydrolysis with hydrochloric acid using established techniques.[42] Conversion of the CNCs to COOH−CNC, by oxidation of the primary alcohol groups to carboxylic acids, was achieved using TEMPO ((2,2,6,6-tetramethylpiperidin-1-yl)oxyl), NaBr and NaClO again following literature procedures.[44] Titration studies[45] on a sample of the CNC determined their charge density to be about 1100 mmol/kg (see Supporting Information Figure S2a). The COOH−CNCs were lyophilized until

dx.doi.org/10.1021/ja4002713 | J. Am. Chem. Soc. 2013, 135, 5167−5174

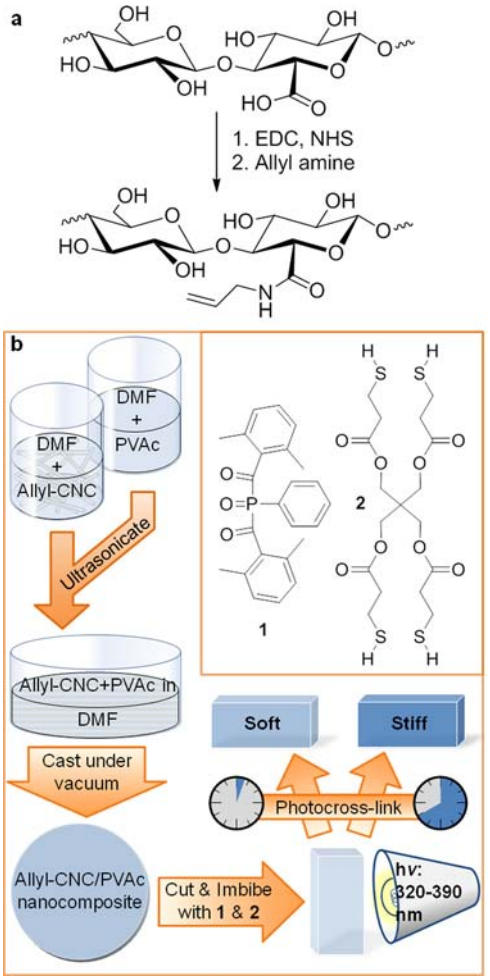

Figure 2. (a) The synthesis of allyl-CNCs and (b) schematic of the film casting and photo-cross-linking process used to access the cross-linked nanocomposite films.

dry and redispersed in dry *N*,*N*-dimethylformamide (DMF) at 5 mg/mL. Covalent attachment of cross-linking functionality was achieved by using standard *N*-hydroxysuccinimide (NHS) peptide coupling procedures.[43] To the stirring COOH−CNC suspension, 5 equiv (relative to the carboxylic acid moieties) of 1-ethyl-3-(3-dimethylaminopropyl) carbodiimide hydrochloride (EDC) was added and stirred for 5 min during which the suspension increased in turbidity. Five equivalents (relative to the carboxylic acid moieties) of NHS was then added to the suspension and the mixture stirred for a further 30 min, during which turbidity dramatically decreased. To this suspension, 10 equivalents of allylamine (relative to the carboxylic acid moieties) was added and the reaction was allowed to stir for 12 h. The reaction was then diluted to 10× volume with deionized water and the modified CNCs (allyl-CNCs) were recovered via centrifugation. The allyl-CNCs were then washed three times with deionized water and dialyzed against deionized water until neutral pH was achieved. Dry allyl-CNCs were then recovered via lyophilization and titrated as before (see Supporting Information Figure S2b) to yield a residual charge density of ca. 200 mmol/kg, consistent with the presence of ca. 900 mmol/kg of allyl groups on the allyl-CNC surface. FT-IR studies were conducted by incorporating CNCs into a KBr pellet and spectra were recorded with an ABB Bomem MB series spectrometer (see Supporting Information Figure S3).

Fabrication of Allyl-CNC Nanocomposites. A stock solution of PVAc (50 mg/mL) in DMF was prepared via stirring, while a stock suspension of allyl-CNCs (2 mg/mL) in DMF was prepared by ultrasonication (ca. 3 h). The nanocomposites were produced by mixing the appropriate ratios of matrix and filler solution/suspension and ultrasonicating for approximately 30 min before casting into PTFE dishes. The DMF was fully removed by placing samples in a vacuum oven under reduced pressure (75 Torr) at room temperature for 24 h. Pressure was reduced further to 20 Torr and the oven was then heated to 40 °C for 120 h. Thermogravimetric analysis (TGA) of the resulting films confirmed that all the DMF had been removed. It is important to note that models utilized to calculate the theoretical modulus of fiber nanocomposites (see Supporting Information) use the volume fraction of the nanofiller to estimate its reinforcement capability; therefore, the descriptions of the nanocomposite samples in figures and discussion are adjusted from wt % to vol % where appropriate (with the densities of PVAc and CNCs as 1.19 and 1.49 g/cm^3, respectively; i.e., 2 wt % is equivalent to 1.6 vol %, 5 wt % is 4.0 vol %, 10 wt % is 8.2 vol %, 15 wt % is 12.4 vol % and 20 wt % is 16.7 vol %).

Imbibing Process. The following preparatory steps were performed under subdued light conditions and annealing/drying steps were performed with the exclusion of light. The appropriate amounts of photoinitiator (Irgacure 819, **1**) (at 5 mol % of total allyl groups) and tetrathiol cross-linker (pentaerythritol tetrakis (3-mercaptopropionate), **2**) (at 25 mol % of total allyl groups to give 1:1 allyl:thiol moieties) were calculated relative to the molar amount of allyl groups within each nanocomposite to be cross-linked. The appropriate volumes of stock 0.1 M DCM solutions of **1** and **2** were measured and combined and this co-solution was further diluted with DCM to give a total volume of ca. 250 μL to make it easier to add to the film. It is important to note that final concentration of this co-solution is different for each nanocomposite sample as the amount of allyl groups in each nanocomposite depends on the film size and CNC loading. Each film was then supported on a PTFE casting dish and the cross-linking co-solution was slowly and evenly pipetted onto the film until the solution was absorbed. Films were then solvent-annealed for 24 h in a saturated atmosphere of DCM at room temperature. Finally, the samples were dried for a further 24 h at room temperature under reduced pressure (ultimately 20 Torr after slowly ramping down from ambient pressure over ca. 3 h so as not to generate solvent vapor bubbles).

Photo-Cross-Linking Process. All films were irradiated with 320−390 nm light at an intensity of 60 mW/cm^2 for times ranging from 2 to 40 min. The films were turned over at the midpoint of the exposure time so both sides of the films were exposed for the same amount of time to promote even distribution of cross-linking throughout the films' thicknesses. The UV-irradiated films were then soaked in 2-propanol for 30 min to remove any unreacted cross-linking reagents. This step was repeated twice with fresh 2-propanol before films were placed in a vacuum oven at room temperature as pressure was slowly reduced from ambient to 20 Torr over ca. 3 h. The temperature was raised to 35 °C for the subsequent 24 h to obtain dry cross-linked films. The removal of all the solvent was confirmed by TGA.

Water Swelling of Nanocomposites. The masses of dry nanocomposite samples were collected before they were placed in vials of DI water which were then placed in a temperature-controlled water bath at 37 °C for 18 h. Samples were blotted dry to remove surface water and wet masses obtained for water swelling calculation. TGA was also used to confirm results. The degree of swelling was calculated by the following equation:

$$\frac{\text{Wet Mass} - \text{Dry Mass}}{\text{Dry Mass}} \times 100 = \%\ \text{Swelling}$$

RESULTS AND DISCUSSION

To access alkene functionalized CNCs, we first isolated tunicate CNCs via hydrochloric acid hydrolysis of the tunicate mantles.[45] The primary OH groups on these uncharged CNCs were then oxidized using literature procedures (TEMPO, NaBr and NaClO)[44] to yield carboxylic acid functionalized CNCs with a charge density of 1100 mmol/kg. The alkene moiety (allyl amine) was reacted with the surface

dx.doi.org/10.1021/ja4002713 | J. Am. Chem. Soc. 2013, 135, 5167−5174

carboxylic acid moieties on the COOH−CNCs using peptide coupling conditions similar to those we previously reported for CNC functionalization. These reaction conditions did not significantly impact the size and dimensions of the CNCs (width ca. 20 nm, length ca. 1800 nm, see Supporting Information for details and Figure S1 for TEM image) during functionalization.[43] Titration studies (see Supporting Information Figure S2b) on the allyl-CNCs showed that they had a residual charge of approximately 200 mmol/kg suggesting that ca. 80% of the carboxylic acid groups were functionalized with the allyl amine. The presence of some residual charge on the allyl-CNCs enables processing by facilitating the dispersion of the nanoparticles in solution. FT-IR studies (see Supporting Information Figure S3) on the COOH−CNCs before functionalization show the presence of a carbonyl stretching peak at 1718 cm^{-1}, which is associated with carboxylic acid moieties. The formation of the amide bond is confirmed by a shift in the carbonyl stretching peak to 1617 cm^{-1} and the appearance of a peak at 1569 cm^{-1} (N−H bending) after functionalization. Furthermore, a shoulder peak at 891 cm^{-1} is consistent with the presence of a terminal alkene group.

The allyl-CNCs were then dispersed in DMF and mixed with varying ratios of PVAc in DMF to yield a series of optically clear nanocomposite films (spanning 2 − 20 wt.%) after solution casting and solvent removal under carefully controlled vacuum conditions (see Supporting Information Figure S4). Thermogravimetric analysis (TGA) was carried out on the films to confirm the removal of solvent. Addition of these films to water resulted in them becoming opaque (see Supporting Information Figure S4) similar to what we have seen in previous systems.[21] Mechanical testing of these nanocomposites in both the dry and wet states was conducted to examine the degree of mechanical reinforcement furnished by this functionalized nanofiller and to confirm that these allyl-CNC nanocomposites display mechanical adaptability upon exposure to water (see Supporting Information Figures S5 and S6). Figure 3 shows the effect on the tensile storage modulus (E') that the volume fraction of CNCs has on both the dry and wet nanocomposites above the T_g of the matrix as measured by dynamic mechanical thermal analysis (DMA). It should be noted that the T_g of the PVAc matrix is only slightly impacted by the presence of CNC filler from ca. 45 °C to ca. 55 °C. However, during the submersion DMA experiments, water absorption plasticizes the PVAc matrix and decreases the T_g of wet nanocomposites to ca. 20 °C.

As we have seen with previous CNC nanocomposites, comparison of the modulus (above the T_g) of the dry and wet nanocomposites at a given volume fraction of CNCs shows that there is a significant drop in modulus upon submersion in water, e.g., the 15 wt % (dry) nanocomposite switches from 599 MPa (dry, at 80 °C) to 31 MPa (wet, at 37 °C). It is important to note that the nanocomposites swell with water, which changes the relative volume fraction of CNC upon immersion in water. As we have observed in similar PVAc/CNC nanocomposites that incorporate sulfonated CNCs[46] (with a surface charge of approximately 85 mmol/kg), the amount of water absorbed by the films increases with increasing CNC content, as can be seen in Figure 3, inset. However, while displaying the same increasing trend in water swelling, the allyl-CNC/PVAc nanocomposites absorb about 60% less water at 37 °C than sulfonate-CNC/PVAc nanocomposites for a given CNC weight percentage. This difference could be attributed to the different surface charged moieties (COOH versus

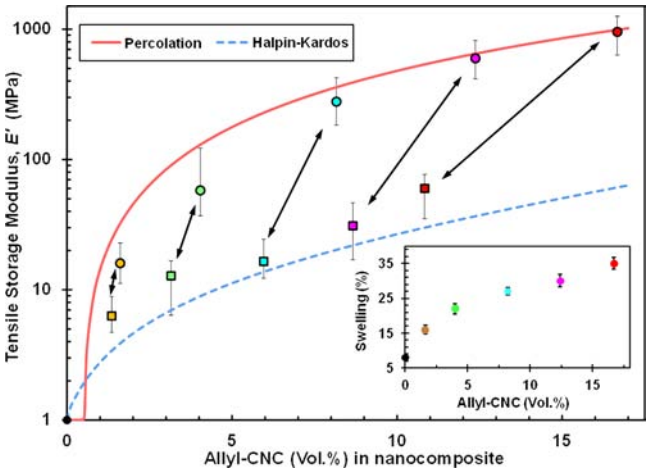

Figure 3. Tensile storage modulus (as measured by DMA) of dry (circles) and wet (squares) uncross-linked allyl-CNC/PVAc nanocomposites 80 and 37 °C, respectively (i.e., 15−25 °C above the T_g of the matrix) as a function of vol % of CNC in the PVAc matrix. Also shown for comparison are the curves for the percolation model (red solid line) and the Halpin-Kardos model (blue dashed line) used to model the dry and wet nanocomposites, respectively. Note: Swelling measurement error is approximately 1 wt % for all samples. Inset: Water swelling measurements at 37 °C for each vol % CNC nanocomposite. The actual modulus data can be found in Supporting Information Table S1.

sulfonate) and/or the presence of relatively hydrophobic allyl groups on the allyl-CNC surfaces. Figure 3 also compares the results to two different theoretical models (see Supporting Information for details) which calculate the mechanical properties of the film as rigid rod-like fillers are incorporated into a polymer matrix (above the T_g) under two distinct conditions. The percolation model (solid red line),[47,48] which assumes the presence of strong interactions between individual nanofiller particles allowing mechanical stress to be transferred along the percolating filler network, describes the dry nanocomposite data at 80 °C (circles) well. The wet data at 37 °C (squares), on the other hand, is better modeled by the Halpin-Kardos model (dashed blue line),[49] which excludes filler−filler interactions in predicting the modulus of nanocomposites. Thus the data show that these allyl-CNC PVAc nanocomposites (at this degree of functionalization) do exhibit adaptable mechanical properties similar to what has been observed with sulfonated CNC nanocomposites.

Having confirmed the mechanical softening capability of the allyl-CNC nanocomposites, the next step was to investigate the effect of covalently cross-linking the nanofiber network on the mechanical properties and switching capability of these materials. The first step was to demonstrate that photoinitiated thiol−ene chemistry could be used to cross-link the allyl-CNCs. To this end, neat allyl-CNC films were created by filtering suspensions of allyl-CNCs in DI H_2O and subsequently drying them. One of the films was then imbibed with a photoinitiator (**1**, 5 mol % relative allyl moieties) and a tetra-functional thiol cross-linker (**2**, 25 mol % relative allyl moieties) (see Supporting Information for details). The imbibed film was then exposed to UV radiation (60 mW/cm^2) for 40 min (20 min per side). After washing with 2-propanol and drying both films, the properties of the films were compared. Samples of both films were then immersed in DI H_2O and sonicated for 3 h, conditions known to redisperse the allyl-CNCs. The uncross-

dx.doi.org/10.1021/ja4002713 | J. Am. Chem. Soc. 2013, 135, 5167−5174

linked allyl-CNC film underwent near-total redispersal in the solvent, while the cross-linked thiol−ene CNC film remained intact, consistent with the presence of a percolating covalently cross-linked CNC network. The mechanical properties of the films were then examined. Rectangular sections (approximately 3 mm × 30 mm × 0.1 mm) of the uncross-linked and cross-linked films were prepared and subject to tensile testing. The data revealed (Figure 4) only a small increase in Young's modulus (E_Y) of ca. 16% and a small decrease in the elongation at break (ε_B) of ca. 25% for the dry cross-linked films as compared to the dry uncross-linked CNC films. Tensile testing performed in water revealed that the cross-linked CNC film exhibited an average wet tensile (Young's) modulus of ca. 955 MPa, which is approximately 25−30% of the dry tensile moduli of both the allyl-CNC and thiol−ene CNC sheets. Note the same experiments cannot be carried out on the allyl-CNC film as immersion of this uncross-linked film in water results in a material too weak to undergo tensile testing and will disperse in the water overtime. It is worthy to note that the oxidation of the CNCs necessary for allyl functionalization is selective for the C6 position, and based on the crystal structure of the CNCs (cellulose I), approximately one-third of the hydroxyl groups on the surface are the C6 hydroxymethyl groups. This combined with the relative inefficiencies of the allyl-CNC synthesis (converting uncharged CNCs to COOH−CNCs and functionalization of COOH−CNCs to allyl-CNCs at approximately 80% conversion) means that there are still an abundance of hydrogen-bonding groups on the surface of the allyl-CNCs. Thus, it is not surprising that the wet modulus of the thiol−ene cross-linked CNC sheet is not as large as the corresponding modulus of the dry allyl-CNC sheets, whether covalently cross-linked or not. Taken together, the data are consistent with both the thiol−ene cross-linked and allyl-CNC films forming strongly interacting networks when dry, a reversible noncovalent (presumably hydrogen bonding) network in the case of the neat allyl-CNC film and a covalent network (presumably aided by additional noncovalent interactions) in the case of the thiol−ene CNC films. Upon exposure to water, the noncovalent interactions are "switched off" in both films; however, on account of the covalent cross-linking, the thiol−ene CNC network retains some of its integrity while the allyl-CNC films simply redisperses, exhibiting no physical robustness.

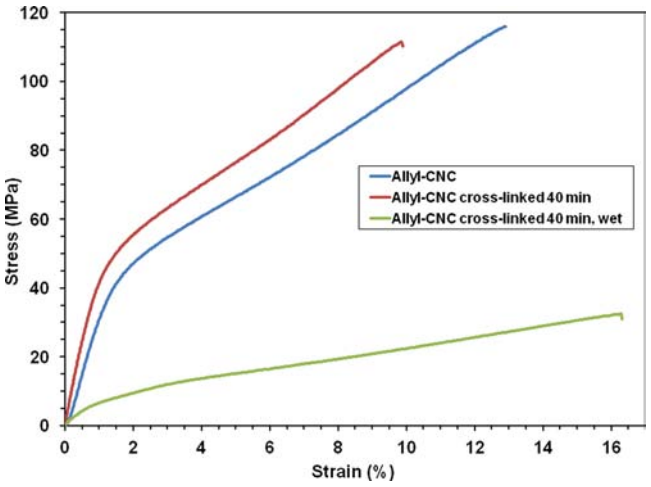

Figure 4. Representative tensile curves for dry sheets of untreated allyl-CNCs, and wet and dry sheet of photo-cross-linked CNCs (irradiated at 60 mW/cm^2 20 min each side). Note: the wet allyl-CNC sheets were not mechanically robust enough to be tensile tested in water and over time eventually form dispersions in the water.

Having demonstrated thiol−ene cross-linking of the allyl-CNCs in standalone films, the next step is to attempt cross-linking the allyl-CNCs within a PVAc matrix. To this end, photoinitiator **1** and tetra-functional thiol cross-linker **2** were imbibed into the nanocomposites in a similar manner to that utilized for the CNC sheets. More specifically, samples were cut from each of the nanocomposites and the total moles of allyl moieties per sample were calculated based on the weight of the sample, the CNC wt %, and the allyl surface coverage on the CNCs (as calculated previously from charge density titrations). The moles of allyl moieties was then used to calculate 5 mol. % of the photoinitiator **1** and 25 mol. % of the tetrafunctional thiol cross-linker **2** (for a 1:20 allyl:photoinitiator ratio and a 1:1 allyl:thiol ratio) for each sample. Then, the appropriate volumes of 0.1 M DCM stock solutions of **1** and **2** were measured, combined, and diluted to approximately 250 μL with DCM before being carefully and evenly absorbed into each film via pipet. Imbibing the photoinitiator and cross-linker after film-casting was necessary to reduce the risk of premature photoinitiation by ambient light or accidental cross-linking due to overheating during the film-casting process. After annealing in a saturated atmosphere of DCM for 18 h, the samples were carefully dried in the dark at room temperature under vacuum. Samples were then exposed to UV-light (60 mW/cm^2) for varying time periods up to 40 min (20 min per side) and immediately immersed in 2-propanol to remove excess and reacted photoinitiator and cross-linker moieties. Two more immersions in fresh 2-propanol were performed and samples were then dried under vacuum for 24 h. TGA was performed to confirm total removal of solvent.

The water swelling ability of the cross-linked nanocomposites was measured for each volume percentage of CNC and irradiation time. Figure 5 shows that a general trend in all the films is decreasing water absorption with increasing irradiation time, consistent with an increase in cross-link density with irradiation time.

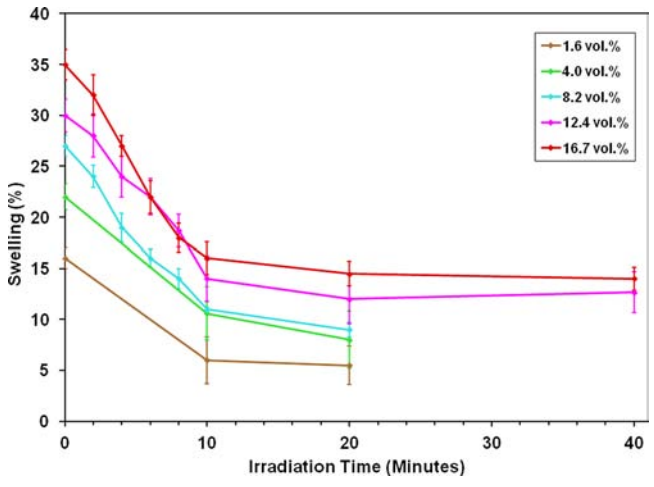

Figure 5. Degree of water swelling versus irradiation time with different vol % CNC nanocomposites, after washing to remove any residual photoinitiator (**1**) and tetrathiol cross-linker (**2**).

dx.doi.org/10.1021/ja4002713 | J. Am. Chem. Soc. 2013, 135, 5167−5174

The mechanical properties of the photo-cross-linked nanocomposites were then evaluated through DMA studies (see Supporting Information Figures S7−S16 for full DMA curves). Figure 6 summarizes all the dry (at 80 °C) and wet (at 37 °C)

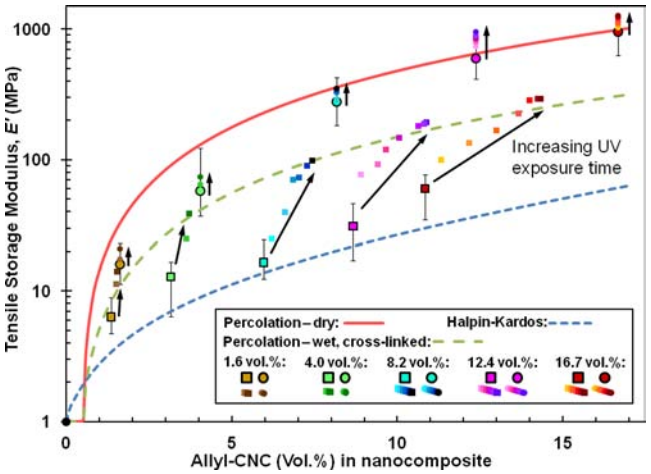

Figure 6. Tensile storage modulus (as measured by DMA) of uncross-linked (black-outlined symbols) and photo-cross-linked (nonoutlined symbols) allyl-CNC/PVAc nanocomposites in both dry at 80 °C (circles) and wet at 37 °C (squares) states. Also shown for comparison are the curves for the percolation model (red solid line), the Halpin-Kardos model (blue, short-dashed line), and the wet, cross-linked percolation model (green long-dashed line) used to model the nanocomposites. Note: Darker colors for cross-linked samples represent longer UV exposure times. The actual modulus data can be found in Supporting Information Table S1.

moduli of all the vol % CNC films highlighting the effect that time of UV exposure has on the tensile storage modulus and water swelling of the nanocomposites. The results clearly show that UV irradiation produces effects consistent with increasing the degree of cross-linking in wet conditions, namely increasing the modulus and decreasing the degree of swelling. The tensile modulus increases with time of UV exposure until the maximum modulus is obtained after ca. 20 min of exposure. The maximum wet modulus obtained is between 20 and 50% of their dry uncross-linked modulus above T_g.

Comparison of the dry tensile storage moduli (E') before and after UV exposure shows only a slight percentage increase in the modulus after cross-linking, with a 10−25% increase in stiffness above the T_g (Supporting Information Table S1a) and ca. 10% increase below T_g (Supporting Information Table S1b). This data is consistent with the presence of a strongly interacting, reinforcing percolating filler network in these dry films with relatively small differences observed between films that have covalent inter-CNC bonds in addition to the noncovalent (hydrogen bonded) CNC network. This agrees with the similar values in the modulus of the cross-linked (thiol−ene CNCs) and uncross-linked allyl-CNC sheets (vide supra). However, comparison of the wet tensile moduli of the uncross-linked and irradiated films at 37 °C (i.e., above wet T_g) shows significant differences. For example, the 20 wt % (in the dry film, 16.7 vol %) CNC shows an increase in wet modulus from 60 MPa to ca. 300 MPa (ca. 500% increase) after 20 min of irradiation. This is consistent with the water being able to disrupt the hydrogen-bonded CNC network in the uncross-linked CNC films but not being able to completely disrupt the covalently cross-linked CNC network. Further confirmation of the cross-linked nature of the photoexposed CNCs in the nanocomposite can be obtained by dissolving away the PVAc matrix in DCM which leaves a thin CNC cross-linked film. In the case of noncross-linked nanocomposites, the remaining CNC film is redispersible in H_2O; however, as seen with the neat thiol−ene CNC film (*vide supra*), the thin CNC film isolated from cross-linked nanocomposites do not redisperse in H_2O (see Supporting Information Figure S18).

Using the wet measured tensile modulus of the thiol−ene cross-linked CNC sheet (955 MPa, vide supra) in the percolation model allows an estimation of the expected modulus of the wet cross-linked nanocomposites (Figure 6, green, long-dashed line). Gratifyingly, the model and our experimental data for the maximally photocross-linked films show agreement. Thus, these results are consistent with the photocross-linking of the CNCs allowing a significant amount of reinforcement to be obtained under wet conditions and that the wet modulus of the nanocomposites can be tuned by simply controlling the amount of light exposure.

Having established the efficacy of the photocross-linking process, the next step was to utilize this process to create mechanical gradient films. This was achieved using a film (20 × 20 × 0.1 mm) containing 15 wt % (12.4 vol %) allyl-CNCs which was homogenously imbibed with **1** and **2** as described previously. The gradient in UV exposure was simply achieved using an aluminum foil mask that was wrapped around 75% of the film, leaving a 5 mm wide strip exposed. The film was then placed under the UV lamp and exposed for 2 min per side (for a total of 4 min of exposure). The mask was then moved to expose 2 mm more of the nanocomposite and irradiated again for 2 min per side. Repeating this procedure three more times gave a film which had sections along its length that have been exposed to a different amount of UV irradiation (0, 4, 8, 12, 16, and 20 min) as shown in Figure 7a. After washing the film with 2-propanol and drying overnight, its gradient properties were then assessed. Samples of the film were cut from the 0, 8, 12, and 20 min irradiated sections and tested by DMA. The E' values for the different cut film strips when dry below and above T_g (25 and 80 °C, respectively) and when wet above T_g (37 °C) are shown in Table 1. As can be seen, an increase in all three of these states is observed with an increase in irradiation time consistent with the increased cross-linking across the length of the film. Perhaps the most striking difference is observed between the three states when the mechanical contrast across the film is examined. The graph in Figure 7a plots the ratio of E' after x minutes of UV exposure to E' of the uncross-linked sample versus exposure time, which highlights the mechanical contrast across the nanocomposite film when dry at 25 and 80 °C and when the film is wet at 37 °C. As can be seen, a dramatic increase in the mechanical contrast is observed for the wet film ($E'_{stiff}/E'_{soft} > 5$) over the dry film either below or above T_g (E'_{stiff}/E'_{soft} of ca. 1.1 and 1.5, respectively). A similar water enhanced mechanical contrast is also observed in the squid beak which exhibits a mechanical contrast ratio of ca. 2 in the dry state (10−5 GPa) to ca. 100 in its natural wet state (5 GPa to 50 MPa). To visually demonstrate the mechanical gradient along the film, a strip of the nanocomposite was cut in parallel with the gradient (so as to include each irradiation increment) and soaked in DI H_2O for 6 h. This gradient film strip is pictured in the top panel of Figure 7b and has a soft to stiff transition from left to right; performing a half twist on this film results in the twist being concentrated at the soft end. In contrast, a uniformly irradiated

dx.doi.org/10.1021/ja4002713 | J. Am. Chem. Soc. 2013, 135, 5167−5174

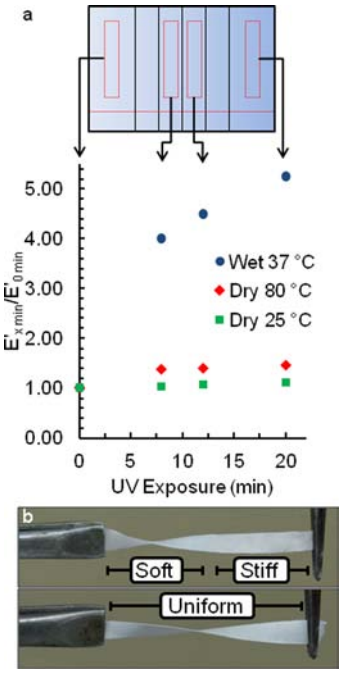

Figure 7. (a) Schematic of the gradient film of 15 wt % (12.4 vol %) allyl-CNCs PVAc nanocomposite with solid lines dividing increments of UV exposure. Red dashed lines represent samples cut out for mechanical testing. The horizontal red long dashed line represents the gradient film sample cut from bottom of film (and shown in the top picture of panel b). Mechanical testing results plotted to highlight the contrast in gradient between the samples dry at 25 °C (green squares), dry at 80 °C (red diamonds), and wet at 37 °C (blue circles). (b) Twisting by half turn of wet nanocomposite samples of a gradient exposed film (top picture, gradient as shown in panel a) and a uniform cross-linked film (bottom picture, 4 min exposure across the length of the film).

Table 1. Tensile Storage Modulus (E') Values for Sections Cut from the Gradient 12.4 vol % CNC/PVAc Film As Measured by DMA

cross-linking time (min)	E', dry 25 °C (MPa)	E', dry 80 °C (MPa)	E', wet 37 °C (MPa)
0	2430	629	36.5
8	2490	859	146
12	2580	881	164
20	2690	912	191

sample (taken from the 4 min irradiated section of the same nanocomposite) shows uniform twisting (bottom panel of Figure 7b) under the same half twist conditions.

CONCLUSIONS

Building on our previous water-responsive, mechanically dynamic nanocomposite studies, we have now shown that the degree of mechanical softening, upon exposure to water, can be simply controlled by altering the degree of cross-linking on the nanofiller component. By using allyl-functionalized CNC/PVAc nanocomposites imbibed with a tetrathiol cross-linker and a UV initiator, the amount of UV exposure (at an intensity of 60 mW/cm^2) can be used to control the degree of cross-linking, with longer exposure times (up to ca. a 20 min limit) resulting in stiffer wet materials. For example, we have shown that the wet modulus of the 20 wt % (16.4 vol %) CNC PVAc film at 37 °C can be increased from ca. 60 MPa to ca. 300 MPa after 20 min of UV cross-linking. This level of reinforcement in the nanocomposites matches up well with the predicted modulus by the percolation theoretical model using the modulus of the reinforcing phase as the wet modulus of the cross-linked CNC sheet. Furthermore, inspired by the squid beak, we have shown that mechanical gradient nanocomposites, that exhibit water-enhanced mechanical contrasts, can be accessed in these films by simply controlling the exposure time of different parts of the film. Thus, this photoinduced cross-linking process should allow access to complex mechanical gradients that can be programmed into a film by using specific photomasks. With such a controllable cross-linking system in hand, the key question arises as to whether stiffer wet CNC nanocomposites can be accessed that would allow larger mechanical contrasts. We are currently undertaking studies to further understand how the degree of allyl functionalization of the CNCs, the ratio of thiol-cross-linker (and photoinitiator) to the allyl-CNCs and the type of thiol cross-linker all impact the wet mechanical properties of the CNC nanocomposites. Another aspect that we are currently investigating is the use of vinyl containing polymer matrices to allow matrix−matrix and CNC−matrix cross-linking in addition to the CNC−CNC cross-linking (which would more closely mimic the proposed cross-linking believed to occur in the squid beak), which would further enhance the wet modulus of the nanocomposite or even switch off the mechanical adaptability of the material altogether. If this can be achieved, then it should be possible to access mechanical gradient films with much larger mechanical contrast than achieved here (E'_{stiff}/E'_{soft} ca. 5) and approach values closer to those which the squid beak exhibits (E_{stiff}/E_{soft} ca. 100).

We see these materials as having broad applications across a number of biomedical applications wherever there is a need to interface stiff therapeutic interventions with a soft biological tissue.[50] For instance, a modulus buffer between the stiff implant and soft tissue would be advantageous to a range of percutaneous technologies, such as glucose sensors for diabetics,[51] osseointegrated prosthetic limbs for amputees,[52] long-term intravascular interfaces such as central venous port systems for chemotherapy,[53] as well as for chronically implanted intracortical microelectrodes.[54−56]

ASSOCIATED CONTENT

Supporting Information

TEM, charge density studies and FT-IR of the COOH- and allyl-CNCs, details of the composite models, tensile testing experiments of CNC films and dynamic mechanical thermal analysis data of all the PVAc/CNC nanocomposites both dry and wet and pictures of dispersion studies of uncross-linked and cross-linked PVAc/CNC films. This material is available free of charge via the Internet at http://pubs.acs.org.

AUTHOR INFORMATION

Corresponding Author

stuart.rowan@case.edu

Notes

The authors declare no competing financial interest.

ACKNOWLEDGMENTS

We thank the NSF-DMR-1204948 and the Kent H. Smith Charitable Trust (S.J.R.) for funding of this project. We would also like to thank the reviewers of this manuscript for their comments which helped to improve and clarify this manuscript.

REFERENCES

(1) Chen, P.-Y.; McKittrick, J.; Meyers, M. A. *Prog. Mater. Sci.* **2012**, *57*, 1492−1704.
(2) Sarikaya, M.; Fong, H.; Frech, D. W.; Humbert, R. *Mater. Sci. Forum* **1999**, *293*, 83−98.
(3) (a) Motokawa, T.; Tsuchi, A. *Biol. Bull.* **2003**, *205*, 261−275. (b) Wilkie, I. C. *J. Exp. Biol.* **2002**, *205*, 159−165. (c) Szulgit, G. K.; Shadwick, R. E. *J. Exp. Biol.* **2000**, *203*, 1539−1550. (d) Koob, T. J.; Koob-Emunds, M. M.; Trotter, J. A. *J. Exp. Biol.* **1999**, *202*, 2291−2301.
(4) Miserez, A.; Schneberk, T.; Sun, C.; Zok, F.; Waite, J. H. *Science* **2008**, *319*, 1816−1819.
(5) Miserez, A.; Li, Y.; Waite, J. H.; Zok, F. *Acta Biomater.* **2007**, *3*, 139−149.
(6) Broonell, C. C.; Khan, R. K.; Moses, D. N.; Miserez, A.; Pontin, M. G.; Stucky, G. D.; Zok, F. W.; Waite, J. H. *J. R. Soc. Interface* **2007**, *4*, 19−31.
(7) Waite, J. H.; Broomell, C. C. *J. Exp. Biol.* **2012**, *215*, 873−883.
(8) Harrington, M. J.; Waite, J. H. *Adv. Mater.* **2009**, *21*, 440−444.
(9) Raabe, D.; Sachs, C.; Romano, P. *Acta Mater.* **2005**, *53*, 4281−4292.
(10) Waite, J. H.; Lichtenegger, H. C.; Stucky, G. D.; Hansma, P. *Biochemistry* **2004**, *43*, 7653−7662.
(11) Zaslansky, P.; Friesem, A. A.; Weiner, S. J. *Struct. Biol.* **2006**, *153*, 188−199.
(12) Marshall, G. W., Jr.; Balooch, M.; Gallagher, R. R.; Gansky, S. A.; Marshall, S. J. *J. Biomed. Mater. Res.* **2001**, *54*, 87−95.
(13) Imbeni, V.; Kruzic, J. J.; Marshall, G. W.; Marshall, S. J.; Ritchie, R. O. *Nat. Mater.* **2005**, *4*, 229−232.
(14) Kryszewski, M. *Polym. Adv. Technol.* **1998**, *9*, 244−259.
(15) Giannakopoulos, A. E.; Suresh, S.; Finot, M.; Olsson, M. *Acta Metall. Mater.* **1995**, *43*, 1335−1354.
(16) Suresh, S. *Science* **2001**, *292*, 2447−2451.
(17) For example, see: (a) Chaudhury, M. K.; Whitesides, G. M. *Science* **1992**, *256*, 1539−1541. (b) Chang, T.; Rozkiewicz, D. I.; Ravoo, B. J.; Meijer, E. W.; Reinhoudt, D. N. *Nano Lett.* **2007**, *7*, 978−980. (c) Genzer, J.; Bhat, R. R. *Langmuir* **2008**, *24*, 2294−2317.
(18) (a) Albert, J. N. L.; Baney, M. J.; Stafford, C. M.; Kelly, J. Y.; Epps, T. H., III. *ACS Nano* **2009**, *3*, 3977−3986. (b) Kelly, J. Y.; Albert, J. N. L.; Howarter, J. A.; Kang, S.; Stafford, C. M.; Epps, T. H., III; Fasolka, M. J. *ACS Appl. Mater. Interfaces* **2010**, *2*, 3241−3248.
(19) Miserez, A.; Rubin, D.; Waite, J. H. *J. Biol. Chem.* **2010**, *285*, 38115−38124.
(20) Hsu, L.; Weder, C.; Rowan, S. J. *J. Mater. Chem.* **2011**, *21*, 2812−2822.
(21) Capadona, J. R.; Shanmuganathan, K.; Tyler, D. J.; Rowan, S. J.; Weder, C. *Science* **2008**, *319*, 1370−1374.
(22) (a) Moon, R. J.; Marini, A.; Nairn, J.; Simonsen, J.; Youngblood, J. *Chem. Soc. Rev.* **2011**, *40*, 3941−3994. (b) Eichhorn, S. J.; Dufresne, A.; Aranguren, M.; Marcovich, N. E.; Capadona, J. R.; Rowan, S. J.; Weder, C.; Thielemans, W.; Roman, M.; Renneckar, S.; Gindl, W.; Veigel, S.; Keckes, J.; Yano, H.; Abe, K.; Nogi, M.; Nakagaito, A. N.; Mangalam, A.; Simonsen, J.; Benight, A. S.; Bismarck, A.; Berglund, L. A.; Peijs, T. *J. Mater. Sci.* **2010**, *45*, 1−33. (c) Habibi, Y.; Lucia, L. A.; Rojas, O. J. *Chem. Rev.* **2010**, *110*, 3479−3500. (d) Eichhorn, S. J. *ACS Macro Lett.* **2012**, *1*, 1237−1239. (e) Tingaut, P.; Zimmerman, T.; Sébe, G. *J. Mater. Chem.* **2012**, *22*, 20105−20111.
(23) (a) Csoka, L.; Hoeger, I. C.; Rojas, O. J.; Peszlen, I.; Pawlak, J. J.; Peralta, P. N. *ACS Macro Lett.* **2012**, *1*, 867−870. (b) Uetani, K.; Yano, H. *ACS Macro Lett.* **2012**, *1*, 651−655. (c) Ma, H.; Burger, C.; Hsiao, B. S.; Chu, B. *ACS Macro Lett.* **2012**, *1*, 213−216. (d) Padalkar, S.; Capadona, J. R.; Rowan, S. J.; Weder, C.; Won, Y. H.; Stanciu, L. A.; Moon, R. J. *J. Mater. Sci.* **2011**, *46*, 5672−5679. (e) Padalkar, S.; Capadona, J. R.; Rowan, S. J.; Weder, C.; Won, Y. H.; Stanciu, L. A.; Moon, R. J. *Langmuir* **2010**, *26*, 8497−8502.
(24) Helbert, W.; Cavaille, J. Y.; Dufresne, A. *Polym. Compos.* **1996**, *17*, 604−611.
(25) Lin, N.; Huang, J.; Dufresne, A. *Nanoscale* **2012**, *11*, 3274−3294.
(26) Azizi Samir, M. A. S.; Alloin, F.; Dufresne, A. *Biomacromolecules* **2005**, *6*, 612−619.
(27) Siró, D.; Plackett, D. *Cellulose* **2010**, *17*, 459−494.
(28) Ben Azouz, K.; Ramires, E. C.; Van den Fonteyne, W.; El Kissi, N.; Dufresne, A. *ACS Macro Lett.* **2012**, *1*, 236−240.
(29) Ma, H.; Burger, C.; Hsiao, B. S.; Chu, B. *ACS Macro Lett.* **2012**, *1*, 723−726.
(30) Fox, J.; Wie, J. J.; Greenland, B. W.; Burattini, S.; Hayes, W.; Colquhoun, H. M.; Mackay, M. E.; Rowan, S. J. *J. Am. Chem. Soc.* **2012**, *134*, 5362−5368.
(31) Fleming, K.; Gray, D.; Prasannan, S.; Matthews, S. *J. Am. Chem. Soc.* **2000**, *122*, 5224−5225.
(32) Woodhams, R. T.; Thomas, G.; Rodgers, D. K. *Polym. Eng. Sci.* **1984**, *24*, 1166−1171.
(33) Siqueira, G.; Bras, J.; Dufresne, A. *Biomacromolecules* **2009**, *10*, 425−432.
(34) Grunert, M.; Winter, W. T. *J. Polym. Environ.* **2002**, *10*, 27−30.
(35) Angles, M. N.; Dufresne, A. *Macromolecules* **2000**, *33*, 8344−8353.
(36) Shanmuganathan, K.; Capadona, J. R.; Rowan, S. J.; Weder, C. *J. Mater. Chem.* **2010**, *20*, 180−186.
(37) Shanmuganathan, K.; Capadona, J. R.; Rowan, S. J.; Weder, C. *ACS Appl. Mater. Interfaces* **2010**, *2*, 165−174.
(38) Dagnon, K. L.; Shanmuganathan, K.; Weder, C.; Rowan, S. J. *Macromolecules* **2012**, *45*, 4707−4715.
(39) Mendez, J.; Annamalai, P. K.; Eichhorn, S. J.; Rusli, R.; Rowan, S. J.; Foster, E.; Weder, C. *Macromolecules* **2011**, *44*, 6827−6835.
(40) Shanmuganathan, K.; Capadona, J. R.; Rowan, S. J.; Weder, C. *J. Mater. Chem.* **2010**, *20*, 180−186.
(41) Capadona, J. R.; Shanmuganathan, K.; Trittschuh, S.; Seidel, S.; Rowan, S. J.; Weder, C. *Biomacromolecules* **2009**, *10*, 712−716.
(42) Rusli, R.; Shanmuganathan, K.; Rowan, S. J.; Weder, C.; Eichhorn, S. J. *Biomacromolecules* **2011**, *12*, 1363−1369.
(43) Way, A. E.; Hsu, L.; Shanmuganathan, K.; Weder, C.; Rowan, S. J. *ACS Macro Lett.* **2012**, *1*, 1001−1006.
(44) Habibi, Y.; Chanzy, H.; Vignon, M. R. *Cellulose* **2006**, *13*, 679−687.
(45) Perez, D. D.; Montanari, S.; Vignon, M. R. *Biomacromolecules* **2003**, *4*, 1417−1425.
(46) Shamnuganathan, K.; Capadona, J. R.; Rowan, S. J.; Weder, C. *Prog. Polym. Sci.* **2010**, *35*, 212−222.
(47) Ouali, N.; Cavaille, J. Y.; Perez, J. *Plast., Rubber Compos. Process. Appl.* **1991**, *16*, 55−60.
(48) Takayanaki, M.; Uemura, S.; Minami, S. *J. Polym. Sci., Part C* **1964**, *5*, 113−122.
(49) Halpin, J. C.; Kardos, J. L. *J. Appl. Phys.* **1972**, *43*, 2235−2241.
(50) Seidi, A.; Ramalingam, M.; Elloumi-Hannachi, I.; Ostrovidov, S.; Khademhosseini, A. *Acta Biomater.* **2011**, *7*, 1441−1451.
(51) (a) Helton, K. L.; Ratner, B. D.; Wisniewski, N. A. *J. Diabetes Sci. Technol.* **2011**, *5*, 632−646. (b) Helton, K. L.; Ratner, B. D.; Wisniewski, N. A. *J. Diabetes Sci. Technol.* **2011**, *5*, 647−56.
(52) (a) Fleckman, P.; Olerud, J. E. *Biomed Mater.* **2008**, *3*, 034006. (b) Pitkin, M. *J. Rehabil. Res. Dev.* **2009**, *46*, 345−360.
(53) Teichgräber, U. K.; Pfitzmann, R.; Hofmann, H. A. *Dtsch. Arztebl. Int.* **2011**, *108*, 147−153.
(54) Gilletti, A.; Muthuswamy, J. *J. Neural Eng.* **2006**, *3*, 189−195.
(55) Capadona, J. R.; Tyler, D. J.; Zorman, C. A.; Rowan, S. J.; Weder, C. *MRS Bull.* **2012**, *37*, 581−589.
(56) (a) Harris, J. P.; Capadona, J. R.; Miller, R. H.; Healy, B. C.; Shanmuganathan, K.; Rowan, S. J.; Weder, C.; Tyler, D. J. *J. Neural Eng.* **2011**, *8*, 066011. (b) Harris, J. P.; Hess, A. E.; Rowan, S. J.; Weder, C.; Zorman, C. A.; Tyler, D. J.; Capadona, J. R. *J. Neural Eng.* **2011**, *8*, 046010. (c) Hess, A. E.; Capadona, J. R.; Shanmuganathan, K.; Rowan, S. J.; Weder, C.; Tyler, D. J.; Zorman, C. A. *J. Micromech. Microeng.* **2011**, *21*, 054009.